Finite element prediction of differential eddy current probe signals from Fe_3O_4 deposits in PWR steam generators

N. Ida, H. Hoshikawa and W. Lord

Finite element analysis techniques have been successfuly applied to the study of eddy current NDT phenomena in axisymmetric test geometries. Major applications of such computer code have related to the design of probes and the gaining of physical insight into just how electromagnetic fields interact with defects. This paper is concerned with an additional application of the code, namely to the simulation of practical testing situations which are too difficult and/or expensive to replicate in a laboratory environment.

Numerical experiments are described which simulate the differential eddy current probe response to the build-up and chemical flushing of magnetite in the crevice gap of a PWR steam generator unit. The simulation results agree well with the only experimental data available to the authors and lead to the conclusion that conventional differential eddy current probes should be capable of characterizing crevice gap conditions with respect to the presence of magnetite.

Keywords: eddy current testing, finite element analysis, magnetite, nuclear reactors

Analysis of the electromagnetic fields associated with eddy current NDT phenomena has to proceed from the quasi-static form of Maxwell's equations

$$\int_c \bar{E} \cdot d\bar{i} = \iint_s \dot{\bar{B}} \cdot d\bar{s} \quad (1)$$

$$\int_c \bar{E} \cdot d\bar{i} = \iint_s \bar{J} \cdot d\bar{s} \quad (2)$$

$$\iint_s \bar{B} \cdot d\bar{s} = 0 \quad (3)$$

and the constitutive relationship

$$\bar{B} = \mu \bar{H} \quad (4)$$

where all the field variables $\bar{E}$, $\bar{B}$, $\bar{H}$ and $\bar{J}$ and phasor vectors because of the sinusoidal nature of eddy current excitation, and μ is a constant only if the material under test is non-ferromagnetic.

The Maxwell-Ampere law of Equation (2) describes the physically observable fact that an alternating current (as in an eddy current probe) sets up an alternating magnetic field. The Maxwell-Faraday law of Equation (1) summarizes many of Faraday's and Henry's observations concerning electromagnetic induction and predicts that if the alternating field of the eddy current probe interacts with a conducting test specimen, an alternating voltage will be induced in the material giving rise to eddy currents. Again by Equation (2), the eddy currents themselves set up an alternating magnetic field which interacts with the excitation probe field, resulting in a change of probe impedance in much the same manner as the load impedance of a transformer is referred into the primary winding.

Phenomonologically then, Equations (1) to (4) are very useful for explaining the basic physics of low frequency electromagnetic field/defect interactions. Unfortunately, one can only progress so far with them in developing analytical expressions for, say, the probe coil impedance given a particular defect shape. The reason for this lies in the very nature of the non-destructive test itself. Material properties, test geometries and the defects and anomalies in them tend not to be describable by simple (or even complex) mathematical expressions. During the past decade, researchers in the NDT and Applied Magnetic Laboratory at Colorado State University have examined the possibility of applying numerical analysis (speci-

0308-9126/85/060331-08 $3.00

fically, finite element methods) to the modelling of electromagnetic field/defect interactions in metals[1].

Starting with active and residual magnetostatic leakage field models[2], the finite element code has now been extended to the study of both steady-state and pulsed eddy current NDT phenomena[3-5]. All of the early code was limited to two-dimensional or axisymmetric test geometries, but recently the magnetostatic and steady-state eddy current code has been converted to a full three-dimensional form[6].

Applications of the eddy current code have centred on the modelling of differential eddy current probe phenomena encountered in the testing of PWR steam generator tubing, particularly in relation to probe design and in developing an understanding of how probe fields interact with steam generator components.

The major purpose of this paper is to describe an additional application of finite element modelling, namely, the prediction of eddy current probe impedance plane trajectories for testing situations that are too difficult to replicate in the laboratory. Such studies are particularly important in the nuclear industry, where the very structure of the components themselves or the operating conditions often preclude the acquisition of required experimental data.

One such situation relates to the build-up of corrosion products (primarily magnetite, Fe_3O_4) in the crevice gaps of PWR steam generators, as shown in Figure 1. Such build-up can ultimately lead to tube denting, requiring the affected tube to be plugged and resulting in an overall loss of steam generator efficiency. Chemical flushing has been suggested as a means to alleviate this problem, and the question naturally arises as to whether a conventional differential eddy current probe is sensitive enough to monitor the process.

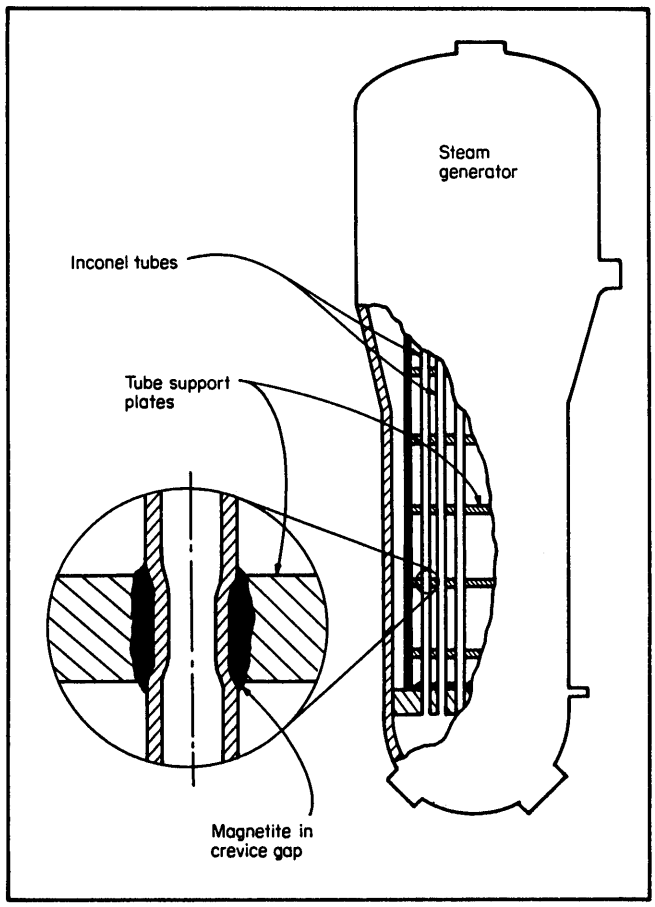

Fig. 1 Schematic diagram of a PWR steam generator

Properties of magnetite

The numerical modelling of geometries containing magnetite poses some unique problems. The first of these is the complete lack of reliable data concerning permeability and conductivity, especially for corrosion products that occur in PWR nuclear power plant steam generators. Thus, for example, Smith and Wijn[7] give a value of 100 for the relative permability and 142.8 Ω^{-1} C^{-1} m^{-1} for conductivity. Snoek[8] gives a value of 70 for relative permeability and the conductivity of magnetite in Landott-Bornstein[9] is 250 Ω^{-1} C^{-1} m^{-1}. These values, all at room temperature, were obtained for Fe_3O_4 crystals (natural or synthetic)[8,9] or pressed material[7] and may or may not be good estimates for the actual material present in steam generators. To compound the problem, corrosion products are a mixture of magnetite and other metals, salts and oxides in a composition that differs from one installation to another and is dependent on the steam generator's construction and water chemistry.

These reasons, and the fact that preliminary numerical calculations indicated a lower permeability than the data given above, prompted an experimental study of the magnetite properties.

Two toroidal samples were prepared by a hot isostatic pressing process. One sample was made of pure magnetite while the other had the following composition (by weight).

74% Fe_3O_4
10% Cu (metallic powder)
10% Cupric oxide
3% Ni (metallic powder)
2% Zn (metallic power)
1% NaCl (powder)

This sample is believed to resemble closely the actual conditions in steam generators and the data obtained were used in the numerical model. The pure magnetite sample was tested for comparison with available data.

Both toroids were subjected to a DC soft magnetic material test[10] using a Hysteresisgraph system to determine their permeability. The results are given in Figure 2, indicating a considerably lower permeability value for the pure magnetite sample in comparison to the literature. The higher permeability of the 'blended' magnetite can be explained as the effective permeability of a mixture[11] and is mainly due to the higher permeability of the nickel.

For the measurement of conductivity, two cylindrical samples of identical materials were prepared. The conductivity was measured using a network analyser. The blended magnetite sample produced a value of 1.6665 Ω^{-1} C^{-1} m^{-1} but no reliable measurement was possible on the pure magnetite sample. This value, however, indicates a conductivity two orders of magnitude lower than that reported in the literature for the pure magnetite.

The finite element model

The partial differential equation governing eddy current phenomena in two-dimensional geometries that include

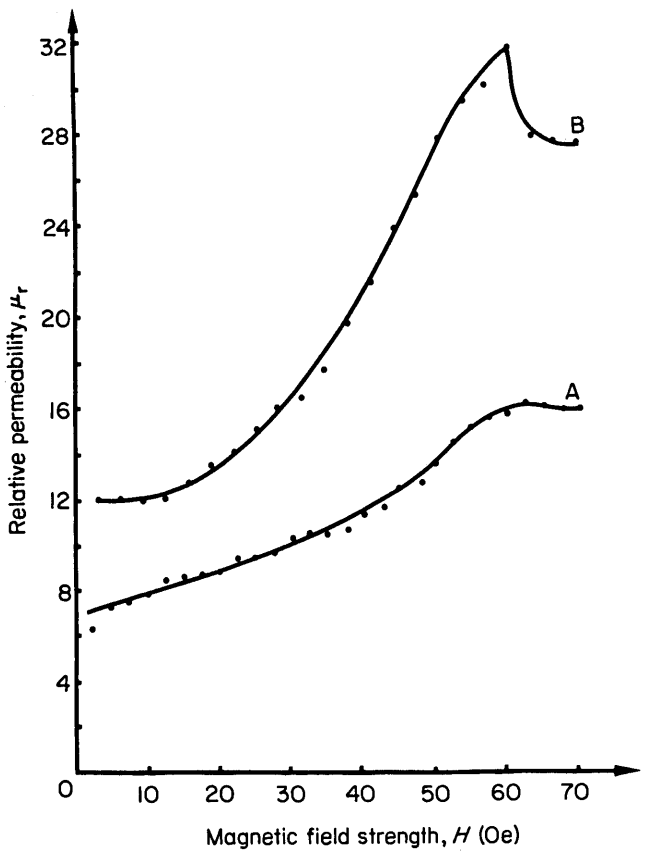

Fig. 2 Relative permeability curves for pure (A) and blended magnetite (B) samples. (1Oe = $1000/4\pi$ A/m^{-1})

conducting and magnetic materials can be written as

$$\frac{1}{\mu}(x\,x\bar{A}) = \bar{J} - \sigma\frac{\partial\bar{A}}{\partial t} \tag{5}$$

where μ, $\bar{A}$, $\bar{J}$ and σ are the magnetic permeability, magnetic vector potential, source current density and electrical conductivity respectively. The derivation of this equation from Maxwell's equation is given elsewhere[12–14] and is not repeated here.

In many practical eddy current NDT situations the geometry is axisymmetric. Such is the case in the testing of steam generator tubing where circular eddy curent coils (absolute or differential) are used. In addition, the excitation for these coils is sinusoidal.

Thus, writing Equation (5) in cylindrical coordinates and performing the differentiation with respect to time for steady-state sinusoidal excitation, a simplified equation is obtained

$$\frac{1}{\mu}\left(\frac{\partial^2\bar{A}}{\partial r^2} + \frac{1}{r}\frac{\partial\bar{A}}{\partial r} + \frac{\partial^2\bar{A}}{\partial z^2} - \frac{\bar{A}^2}{r^2}\right) = -J_s + j\omega\sigma\bar{A} \tag{6}$$

In this system, both J and A are functions of r and z only and have a single component in the positive θ direction.

In the derivation of the above equation, the following assumptions were made.

1. The source current density J_s and the magnetic vector potential A are phasor-vectors. Thus, harmonics are absent in both the impressed and induced fields.
2. Electrical conductivity and magnetic permeability are single valued in each element of the region. Thus, the model is linear and cannot account for field dependency of the permeability, although spatial variation in μ can be modelled.
3. Low frequency operation. The displacement currents as well as volume or surface charges in Maxwell's equations are neglected.
4. Eddy currents within the excitation coils are neglected. This is equivalent to assuming that the AC resistance of the eddy current coils is constant and equal to its DC values.

These assumptions are certainly justified in eddy current NDT applications where the frequency and excitation levels are low.

Equation (6) cannot be solved directly. Instead, the solution region is first discretized into a large number of finite elements of some predetermined shape and the equation formulated for the partiulcar element using any of the number of general methods available for this purpose[15]. The most appropriate method is the use of an energy-related functional which is a statement of energy balance in the solution region. The balance between stored, dissipated and input energy can be written as

$$F(A) = \int_v \left[\frac{1}{\mu}B\mathrm{d}B = j\omega\sigma|A|^2 - J_s\cdot A\right]\mathrm{d}v \tag{7}$$

The solution now consists of finding a set of approximating functions A such that the energy-related functional is minimized. This is done at discrete points in the solution region by solving a system of linear equations derived in the minimization process[14].

From the magnetic vector potential, calculated by the finite element method, one can calculate any derivable magnetic quantities such as field densities and probe impedances.

The impedance of an eddy current probe is calculated from the coils' geometry and the calculated magnetic vector potential. The impedance of a circular loop of radius r_i and carrying an RMS current I_s can be calculated as

$$\bar{z}_i = \frac{j\omega 2\pi r_i\bar{A}_i}{I_s} \tag{8}$$

where $\bar{A}_i$ is the value of the magnetic vector potential at r_i.

Integration of this equation over the cross-section of the coil yields the impedance of the coil. The magnetic vector potential is only known at the nodal points of the finite element mesh, and therefore an average value A_c is calculated at the centroid of each element and assumed constant within the element. The impedance of an absolute eddy current probe then becomes

$$\bar{z} = \frac{j\omega 2\pi\bar{J}_s}{I_s^2}\sum_{i=1}^{N_a}(r_{ci}\Delta_i)\bar{A}_{ci} \tag{9}$$

where r_{ci} is the distance of the centroid of element i from

the symmetry line, J_s is the total current density in the coil ($J_s = N \cdot I_s$, where N is the number of turns in the coil), Δ_i is the area of element i and N_a is the number of finite elements in the cross-section of the coil.

Similarly, the impedance of a differential probe is

$$z = \frac{I\omega 2\pi \bar{J}_s}{I_s^2} \sum_{i=1}^{N_b} (r_{ci}\Delta_i)A_{ci} - \sum_{i=1}^{N_a} (r_{ci}\Delta_i)A_{ci} \qquad (10)$$

where N_a and N_b are the number of elements in the cross-section of the two coils of the probe.

A plot of the complex impedance obtained by Equations (9) or (10) with the real part on the horizontal axis and the imaginary part on the vertical axis is called an 'impedance plane trajectory' and is a common way of representing eddy current test date.

Results

The model described above was applied to a detailed numerical study of magnetite build-up in the crevice gap in PWR steam generators. There is still a significant uncertainty as to the magnetite build-up process itself, since it is not known exactly how the magnetite accumulates in the crevice gap. Similarly, in the chemical flushing process, the magnetite is removed

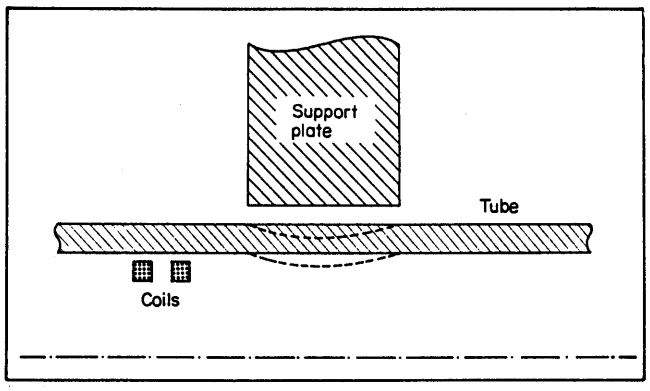

Fig. 3 Crevice gap region in a PWR steam generator

but the signal obtained while monitoring the process depends on the way the magnetite is flushed. In the numerical study, the possibility of radial or axial build-up (or flushing), axial build-up from one side of the support plate, and flushing in the presence of tube denting were modelled, although because of the large number of impedance plane trajectories obtained only representative data are presented in this work.

The geometry considered is presented in Figure 3. It consists of an Inconel 600 tube (22 mm in diameter, 1.3 mm wall thickness) inside a 19 mm carbon steel

Table 1. Material properties used in the finite element studies

	Carbon steel	Inconel	Magnetite
Conductivity, $\sigma(\Omega^{-1}\ m^{-1})$	5.7×10^6	1.1×10^6	166
Relative permeability μ_R	50	1	7

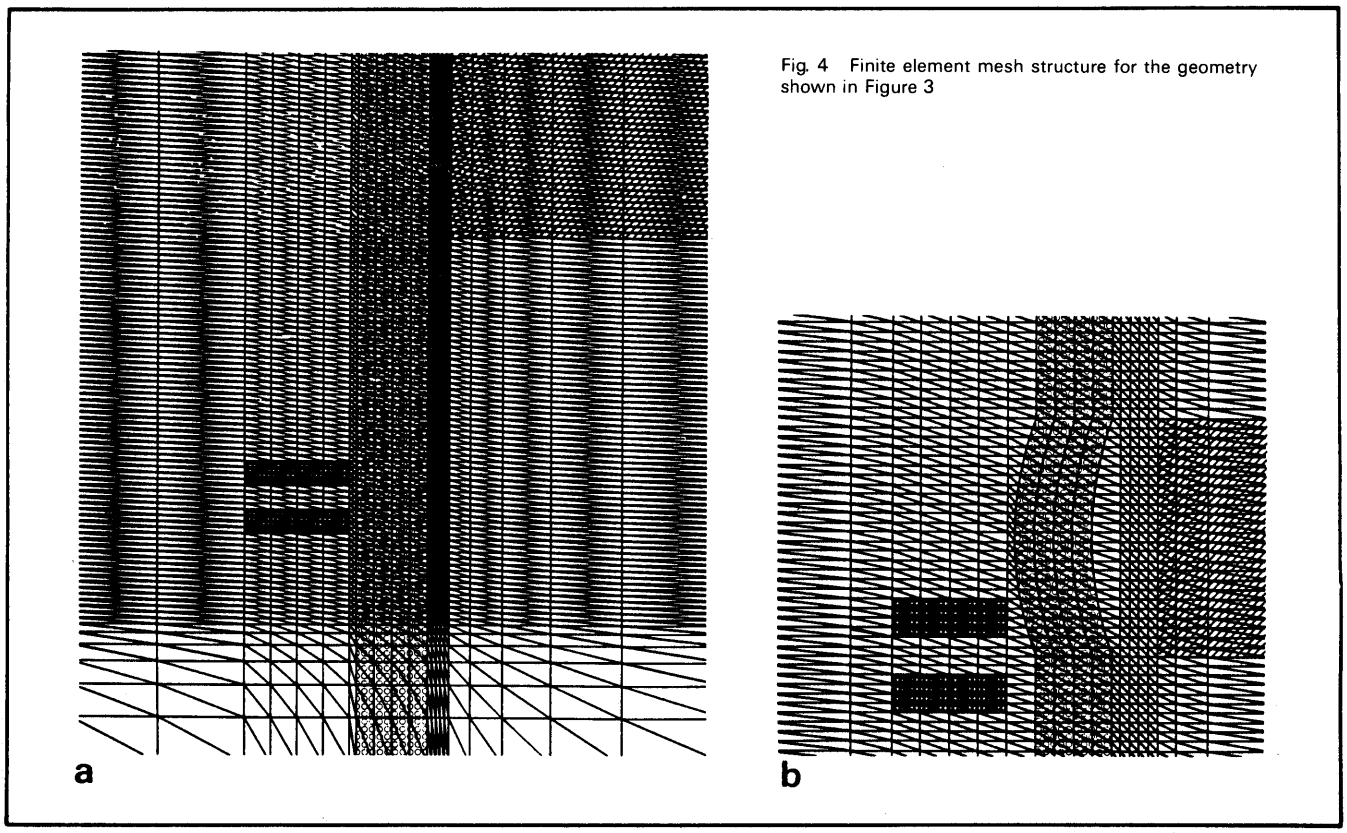

Fig. 4 Finite element mesh structure for the geometry shown in Figure 3

support plate. The crevice gap between the tube and support plate is 0.38 mm while the probe modelled is a differential eddy current probe. The dashed lines represent schematically the area in which denting was modelled. The material properties used are summarized in Table 1.

Figure 4a is the finite element mesh used in the numerical model. Because of symmetry only half the geometry in Figure 3 is modelled. The mesh consists of 13 600 triangular elements and 7035 nodes, resulting in a system of 7035 linear equations with a semi-bandwidth of 37.

The region of probe movement is within the dense mesh portion at the centre of the mesh. This uniformly divided region consists of a total of 180 layers, while the probe is allowed to move for a maximum of 140 probe positions. In some cases, such as the axial build-up study, the geometry is also symmetrical about the centre of the support plate, in which case only 70 probe positions are modelled. Figure 4b shows how the mesh

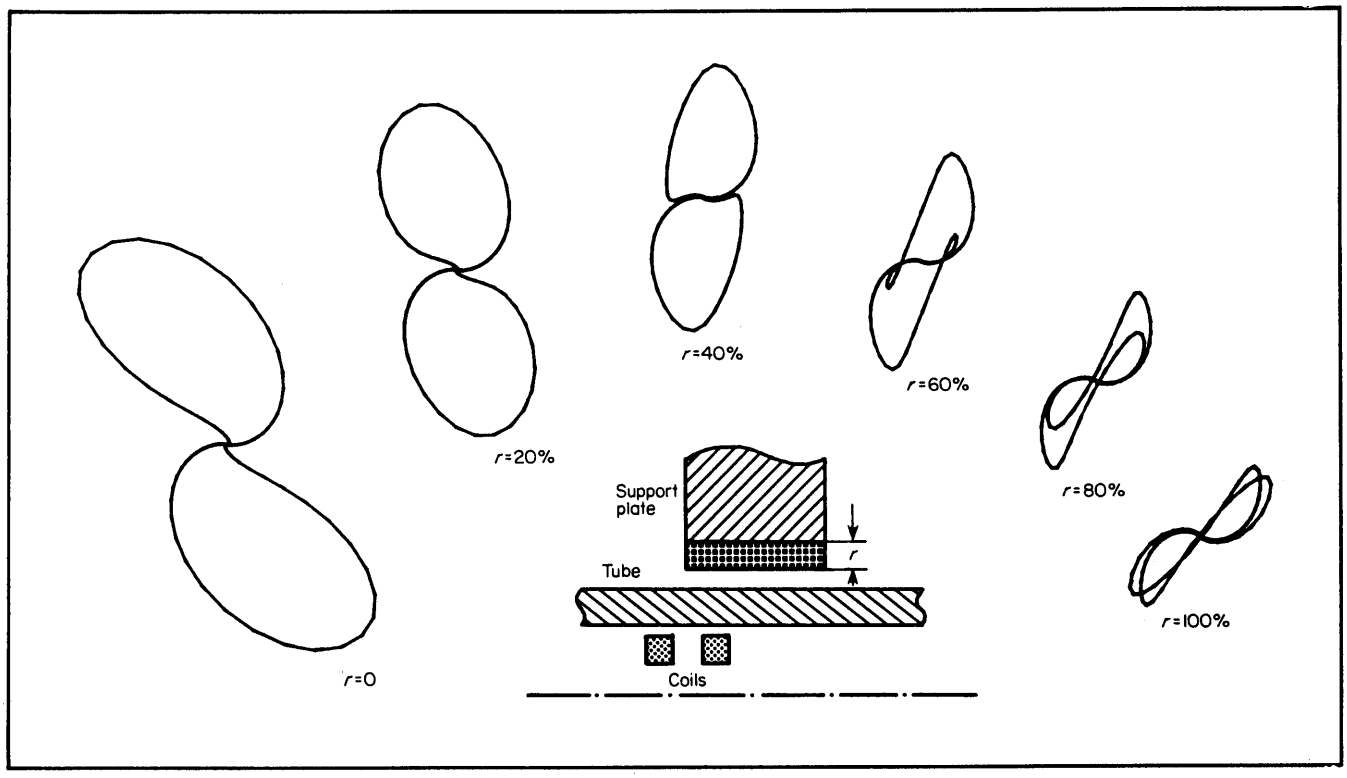

Fig. 5 Finite element predictions of differential probe impedance plane trajectories for radial magnetite build-up

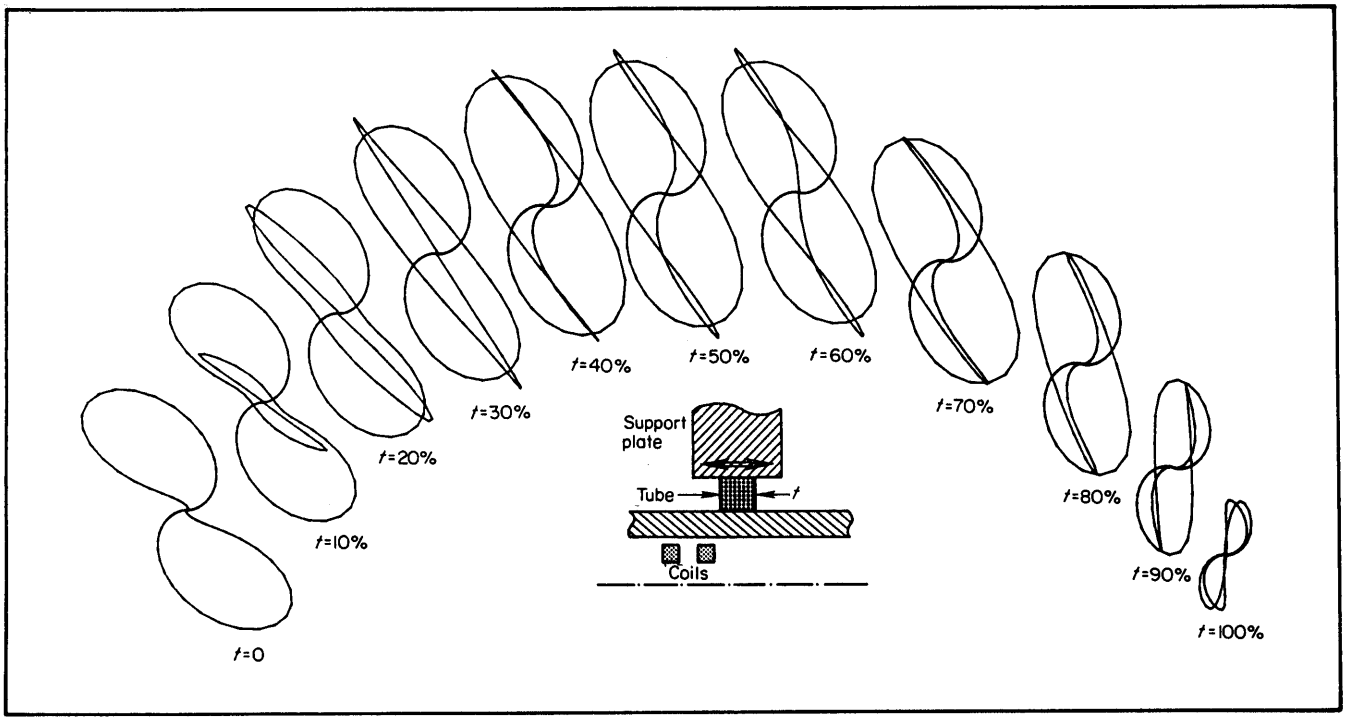

Fig. 6 Finite element predictions of differential probe impedance plane trajectories for axial magnetite build-up

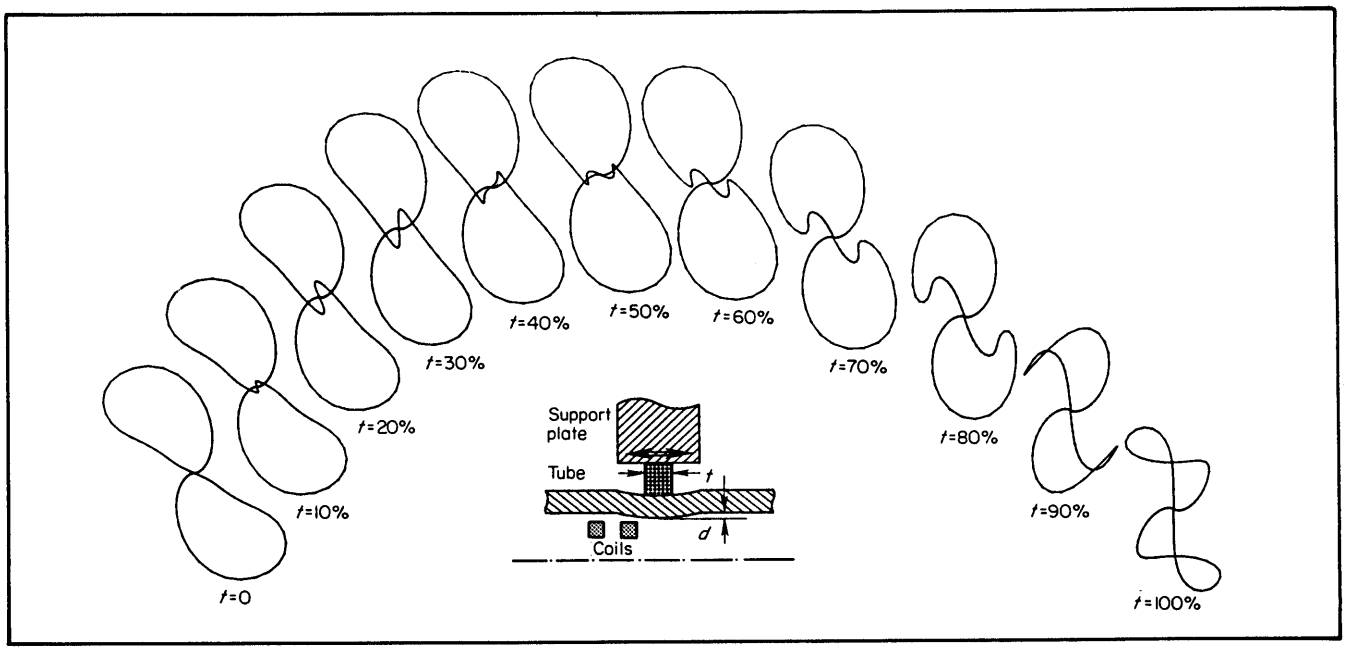

Fig. 7 Finite element predictions of differential probe impedance plane trajectories for axial build-up in the presence of denting. $d = 100$ μm

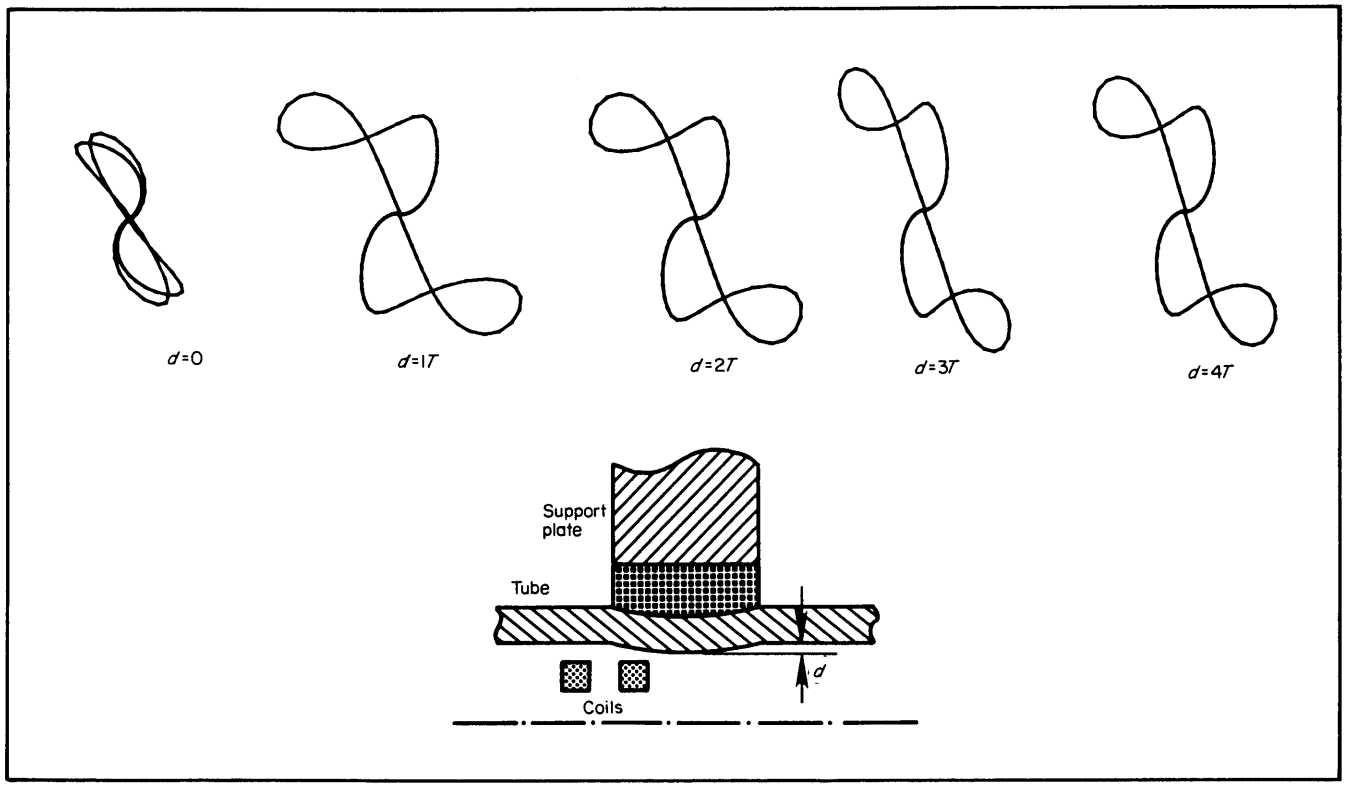

Fig. 8 Effects of denting on probe impedance plane trajectories. $T = 25$ μm

is adjusted in the tube region under the support plate to take into account denting of the tube as well as build-up or flushing of magnetite in the crevice gap over a dented tube.

Here again, for lack of any definite information as to the exact shape of dents in tubes, the dented portion is represented by a circular arc.

The first part of the study deals with radial build-up of magnetite from the support plate towards the tube, or alternatively, the flushing of magnetite from the tube towards the support plate. Figure 5 shows both the geometry involved and the corresponding impedance plane trajectories for magnetite build-up in layers of 76 μm. The change in signal from a clean gap to one full of magnetite is quite dramatic both in shape and magnitude.

The second part of the study assumes an axial build-up of magnetite from the centre of the support plate outwards. Although this is not very likely to happen in the build-up process, it is representative of a chemical flushing process where the chemical agents attack the magnetite from both sides. Figure 6 shows this

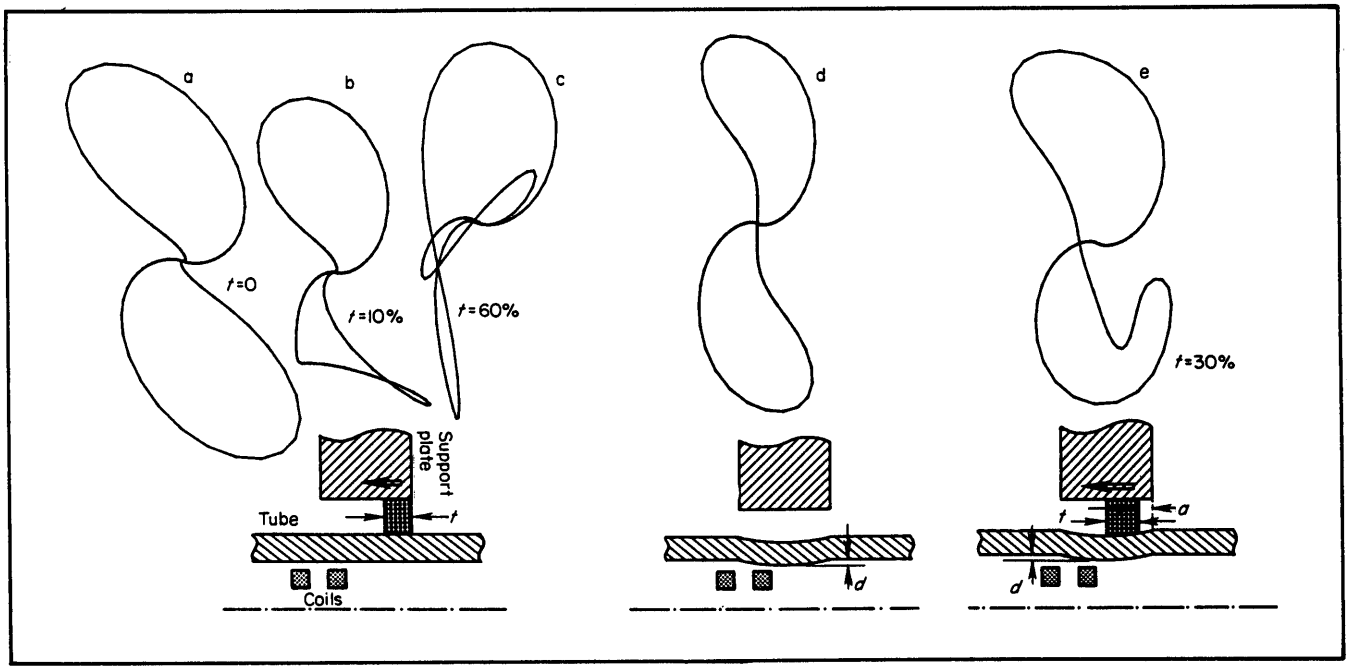

Fig. 9 Comparison of predicted impedance plane trajectories for various crevice gap conditions: a — $t=0$; 6 — $t=10\%$; c — $t=60\%$; d — $d=50$ μm; e — $t=30\%$, $a=10\%$, $d=100$ μm

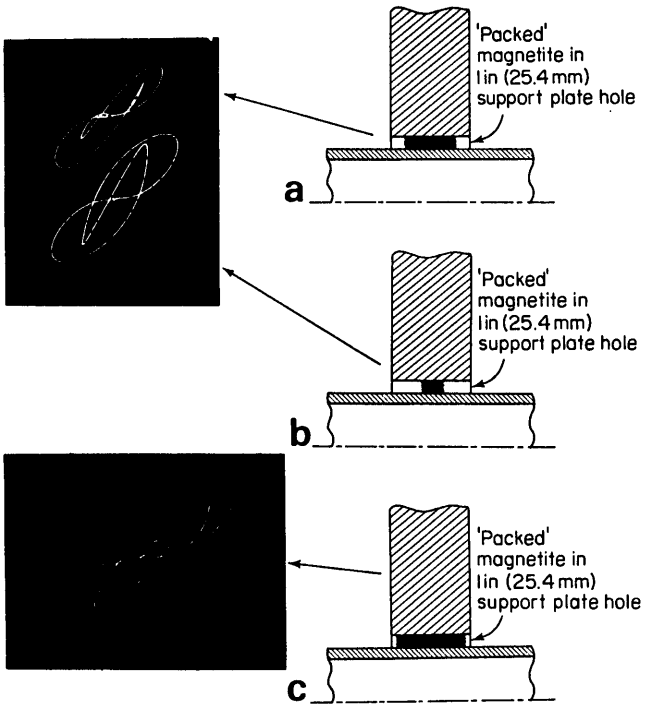

Fig. 10 Experimental results obtained from an enlarged crevice gap packed with pure magnetite

situation and again the changes, especially between a clean support plate and one with magnetite or between a full gap and partially filled gap, are quite dramatic.

Another problem of significant interest in NDT is that of denting of tubes due to magnetite build-up. Similarly, monitoring the flushing of magnetite in this situation is more important to ensure the complete cleaning of the magnetite in the gap.

Figure 7 shows the impedance plane trajectories of axial magnetite build-up (or flushing) in various amounts from a clean gap to a gap full of magnetite. From these plots it is clear that even small amounts of magnetite in the gap give a clear indication.

While in the previous parts of the study there is a clear distinction between the various stages of magnetite build-up, monitoring of the denting process itself seems to be more complicated, as shown in Figure 8. The output for a small dent (25 μm) and a large dent (100 μm) are quite similar. On the other hand, the detection of denting itself is straightforward as indicated by the two leftmost trajectories.

In addition to the data presented above, studies were carried out with axial build-up from one side of the support plate (Figures 9b and 9c), axial build-up from one side of the support plate with a portion of the gap clean on both sides of the magnetite band (Figure 9e) as well as with denting of the tube without the presence of magnetite (Figure 9d). For comparison, the clean crevice gap trajectory is given again in Figure 9a.

Experimental work

Any conceivable geometry (within the limitation of a two-dimensional or axisymmetric model) can be reproduced using the finite element code. There still remains, however, the question of comparison with real, known data. The experimental measurement of a support plate signal in the presence of a clean crevice gap is, of course, only part of the answer. Most of the trajectories in Figures 5 to 9 cannot be reproduced experimentally, because it is impossible to pack a 0.38 mm gap with magnetite, at least certainly not in any controlled manner.

Partly to answer this question, the experiment in Figure 10 was carried out. Here a support plate was drilled to provide a 1.5 mm gap which was then packed

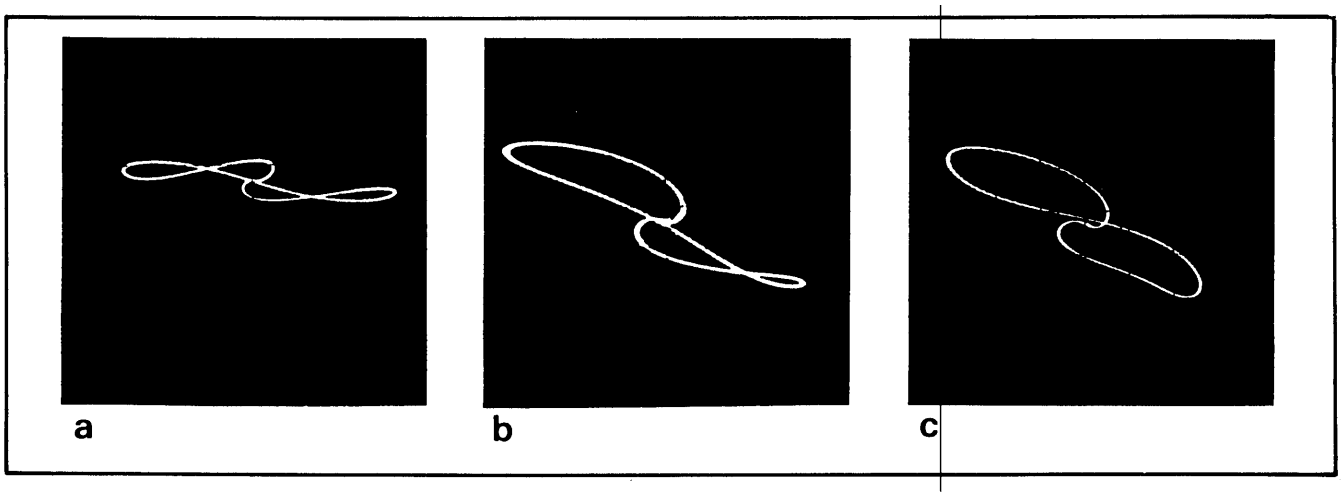

Fig. 11 Results obtained during chemical flushing tests on a model boiler

axially with powdered magnetite at about 60% (Figure 10a), 30% (Figure 10b) and 90% (Figure 10c). The resemblance to the corresponding trajectories in Figure 5 is immediately evident.

More convincing evidence as to the ability, accuracy and usefulness of this model is provided in Figure 11. These impedance plane trajectories were obtained during the chemical flushing of a model boiler. The data are from a tube with a 100 μm dent (radial) at various stages of flushing. Figure 11a was taken before flushing and shows a clearly identifiable dent filled with magnetite. As the flushing progressed, the gap shows various stages of cleaning. Thus, for example, in Figure 11b, one side of the gap is almost completely cleaned as indicated by the single large upper lobe while the rest is still packed with magnetite, indicating an uneven flushing from both sides of the support plate. Figure 11c shows a clean gap while the dent in the tube is visible.

This particular test, besides providing a convincing experimental confirmation of the model, also points out the value of such a tool in interpreting realistic data.

Conclusions

This paper describes a unique application of axisymmetric finite element code to the simulation of an eddy current NDT situation too complex to replicate experimentally. Results of the modelling study clearly show the sensitivity of a conventional, differential eddy current probe to conditions in the crevice gaps of PWR steam generators during magnetite build-up and flushing. Limited experimental data seem to confirm the theoretical predictions.

Acknowledgement

This work has been supported by the Electric Power Research Institute under contract RP 1395-2.

Authors

N. Ida is with the University of Akron, USA, H. Hoshikawa with Nihon University, Japan, and W. Lord with Colorado State University, USA.

References

1 **Lord, W.** 'Applications of numerical modeling to electromagnetic methods of nondestructive testing' *IEEE Trans Magnetics* **MAG-19,** No. 6 (Nov 1983) pp 2437-2442
2 **Lord, W. and Huang, J.H.** 'Defect characterization from magnetic leakage fields' *Brit J Nondestr Testing* **19,** No. 1, (Jan 17, 1977) pp 14-18
3 **Ida N., Palanisamy, R. and Lord, W.** 'Eddy current probe design using finite element analysis' *Mater Eval* **41** No. 12 (Nov 1983) pp 1389-1394
4 **Ida, N. and Lord, W.** 'Graphical simulation of electromagnetic NDT probe fields' *IEEE Computer Graphics Appl* (May/June 1983) pp 21-28
5 **Allen, B. and Lord, W.** 'Finite element modeling of pulsed eddy current phenomena' in *Review of Progress in Quantitative Nondestructive Evaluation,* D.O. Thompson and D.E. Chimenti, Eds., Plenum (1984) pp 561-568
6 **Ida, N. and Lord, W.** '3-D finite element prediction of magnetostatic leakage fields' *IEEE Trans Magnetics* **MAG-19** No 5 (Sept 1983) pp 2260-2265
7 **Smith, J. and Wijn, H.P.J.** *Ferrites* Wiley, Inc., New York (1959) p 229 and p 251
8 **Snoek, J.L.** (Ed.) *New Developments in Ferromagnetic Materials* Elsevier New York (1947) Ch. I.
9 **Landott and Boernstein** *Zahlen und Funktionen* Vol. II, Springer Verlag, Berlin (1962)
10 ASTM - 'Direct current magnetic measurements for soft magnetic materials' *ASTM special publication* 371 sl, ASTM, Philadelphia (1970)
11 **Brown, W.F.** 'Magnetostatic principles in ferromagnetism' in *Selected Topics in Solid State Physics* Vol. 1, Ed. E.P. Wohlfarth, North-Holland Publishing Co., New York
12 **Anderson, O.W.** 'Transformer leakage flux program based on the finite element method' *IEEE Trans Power Apparatus and Systems* **92** (Mar-Apr 1973), pp 682-689
13 **Palanisamy, R. and Lord, W.** 'Finite element modeling of electromagnetic NDT phenomena' *IEEE Trans Magnetics* **MAG-15** No 6 (1979) pp 1479-1481
14 **Ida, N., Betzold, K. and Lord, W.** 'Finite element modeling of absolute eddy current probe signals' *J Nondestr Eval* **3,** No. 3 (1983) pp 147-154
15 **Huebner, K.H.** *The Finite Element Method for Engineers* John Wiley and Sons, New York (1975)

Paper received 29 May 1985. Revised 15 August 1985